Magnetic interactions in 3*d* metal chains on $Cu_2X/Cu(001)$ (X = N, O): Comparison with corresponding unsupported chains

M. C. Urdaniz,[1] M. A. Barral,[1,2] A. M. Llois,[1,2] and A. Saúl[3,4,5]

[1]*Departamento de Física, Comisión Nacional de Energía Atómica, Gral. Paz 1499, 1650 San Martín, Buenos Aires, Argentina*

[2]*Departamento de Física "Juan José Giambiagi," Facultad de Ciencias Exactas y Naturales, Universidad de Buenos Aires, Ciudad Universitaria, Pabellón I, 1428 Buenos Aires, Argentina*

[3]*CINaM, Université d'Aix Marseille-CNRS, Campus de Luminy, case 913, 13288 Marseille Cedex 9, France*

[4]*Department of Civil and Environmental Engineering, Massachusetts Institute of Technology, 77 Massachusetts Avenue, Cambridge, Massachusetts 02139, USA*

[5]*MultiScale Material Science for Energy and Environment, UMI 3466 CNRS-MIT, 77 Massachusetts Avenue, Cambridge, Massachusetts 02139, USA*

(Received 10 July 2014; revised manuscript received 29 October 2014; published 18 November 2014)

In this work we present a systematic study of the magnetic interactions within 3*d* transition-metal chains adsorbed on Cu_2N and Cu_2O monolayers grown on Cu(001). We are interested in the particular geometric adsorption configuration which gives rise, after relaxation, to the development of diatomic TM-X (X = N, O) chains. By using density functional theory (DFT), we calculate the energy difference between the ferromagnetic and antiferromagnetic intrachain configurations for Ti, V, Cr, Mn, Fe, and Co. Both substrates give rise, with minor differences, to the same magnetic trends, the only chains which are ferromagnetic after adsorption are Cr chains. By performing similar calculations in unsupported chains and introducing a tight-binding-model Hamiltonian based on physically reasonable assumptions we reproduce the magnetic trends obtained from the DFT calculations.

DOI: 10.1103/PhysRevB.90.195423 PACS number(s): 75.75.−c, 73.22.−f

I. INTRODUCTION

During many years, experimental work in low-dimensional magnetism relied on the existence of crystalline samples formed by periodic arrangements of the desired low-dimensional systems. It has been possible to study the magnetic properties of thermodynamic ensembles of dimers [1–4], trimers [5,6], linear chains [7–9], or ladders [10,11]. Advances in surface-physics methods during the past decades allowed to study the magnetic properties of ensembles [12,13] and individual [14–23] deposited structures.

For example, x-ray magnetic circular dichroism (XMCD) was used to study the magnetic properties of one-dimensional (1D) Co chains grown by ultrahigh vacuum deposition on a vicinal Pt(997) surface [12,13].

By using a low-temperature, high-magnetic-field scanning tunneling microscope, Heinrich *et al.* [14] have studied spin-excitation spectra of single Mn atoms deposited on Al_2O_3 islands on a NiAl surface. Hirjibehedin *et al.* [15–17] measured the magnetic ground state of Mn chains adsorbed on two different sites of a substrate formed by a decoupling monolayer of copper nitride Cu_2N deposited on Cu(001). Loth *et al.* used the spin-polarized current of a scanning tunneling microscope to modify and measure the spin state of Mn atoms and dimers [20] and finite Fe chains [23] on the same $Cu_2N/Cu(001)$ substrate. It has also been shown that the magnetocrystalline anisotropy of a single Fe atom deposited on the same substrate depends on the relative position of the other nearby Fe atoms [24].

Several groups have performed calculations based on density functional theory (DFT) to study the magnetic properties of free-standing or deposited low-dimensional systems [16,25–28].

Mokrousov *et al.* considered a series of 3*d* transition metals deposited on different substrates [Cu, Pd, Ag, and NiAl(110)] [25]. Rudenko *et al.* studied the magnetic interactions and anisotropies of the experimentally observed Mn chains on $Cu_2N/Cu(001)$ [26]. Urdaniz *et al.* recently considered possible adsorption sites other than the experimentally reported ones for 3*d* transition-metal (TM) chains on $Cu_2N/Cu(001)$. By performing total-energy calculations based on DFT, they concluded that different magnetic-interaction mechanisms can exist depending on the geometry [28]. In the present work, we focus on one of these configurations: the one which is the energetically most favorable and, namely, one of the two possibilities experimentally achieved in the case of Mn chains [15,16]. For this geometry we assume that 3*d* atoms, from Ti to Co, are atomically manipulated and deposited on top of Cu atoms of the underlying copper nitride Cu_2N monolayer along the direction determined by the nearest-neighbor N atoms. The deposited atoms, together with the neighboring nitrogen atoms, end up building diatomic chains, as has been shown in previous papers [16,28].

Within this arrangement, our calculations based on DFT show that the magnetic ground state as a function of *d* filling goes from nonmagnetic to ferromagnetic in the middle of the 3*d* series and to antiferromagnetic at the end of it. This behavior contrasts with the calculated ferromagnetic ground state of free-standing 3*d* transition-metal chains of V, Cr, Mn, Fe, and Co at the same distance [25]. This demonstrates that the substrate as well as the *d* filling of the adsorbed transition-metal atoms both play a role in the determination of the nature of the magnetic interaction. To try to separate both effects, we perform calculations where the decoupling monolayer contains oxygen instead of nitrogen and compare the magnetic properties for both substrates. The idea of replacing nitrogen by oxygen is not only to study the effect

of including one more electron (which is already taken into account by the series of 3*d* TMs studied) but to understand the consequence of using a decoupling monolayer with a more electronegative ligand.

We also compare the magnetic ground state of free-standing (unsupported) TM-O and TM-N chains with the same interatomic distance and we estimate the kinetic exchange contributions of the different bands to the magnetic order using a tight-binding Hamiltonian. We show that the use of a simple set of parameters and the application of physically reasonable assumptions can account for the observed magnetic trends.

In Sec. II we describe the calculation details and the system of interest. In Sec. III we present the results of the ground-state energies for the TM chains on Cu_2N/Cu(001) and Cu_2O/Cu(001) substrates and the unsupported TM-N and TM-O chains. We then introduce the model Hamiltonian and the expressions for the exchange energy of the different orbital contributions in Sec. IV. We finally discuss and conclude in Sec. V.

II. CALCULATION DETAILS AND DESCRIPTION OF SYSTEMS

In order to study the electronic and magnetic properties of the TM chains deposited on Cu_2N/Cu(001) and Cu_2O/Cu(001), we carry out DFT calculations by using the full potential linearized augmented plane waves method (FP-LAPW), as implemented in the WIEN2k code [29]. The generalized gradient approximation (GGA) for the exchange and correlation potential in the parametrization of Perdew, Burke, and Ernzerhof [30] and the augmented plane waves local orbital (apw-lo) basis are used. The cutoff parameter which gives the number of plane waves in the interstitial region is taken as $R_{\mathrm{MT}}K_{\mathrm{max}} = 7$, where K_{max} is the value of the largest reciprocal lattice vector used in the plane waves' expansion and R_{MT} is the smallest *muffin tin* radius used. The number of $\vec{k}$ points in the Brillouin zone is enough in each case to obtain the desired energy and charge precision; namely, 10^{-4} Ry and $10^{-4}e$, respectively.

Cu(001) is modeled by using a periodic supercell composed by a five-layer slab and a vacuum region of 13.8 Å. The thickness of the vacuum region is found to be sufficiently large to avoid interactions among subsequent slabs. The N and O atoms are adsorbed in a $c(2 \times 2)$ configuration in the fourfold-coordinated hollow sites on the outermost metallic copper layer. To exploit inversion symmetry and to prevent unphysical multipoles, each slab has one Cu_2N or one Cu_2O monolayer on each side. We use the experimental lattice constant of copper, which is only 0.27% smaller than the corresponding one obtained with GGA-DFT for bulk Cu.

In the calculations, we consider that the adsorbed 3*d* atomic chains are infinitely long and are deposited on both sides of the slabs. In the adsorption geometry studied, the 3*d* atoms are arranged directly on top of Cu atoms of the Cu_2N [Figs. 1(a) and 1(b)] or Cu_2O [Figs. 1(c) and 1(d)] monolayer, in such a way that one *sp* atom lies between each pair of 3*d* atoms along the chain. There are four lateral copper atoms of the Cu_2N or Cu_2O monolayer surrounding each chain atom and the nearest-neighbor $3d-3d$ distance along the chains is 3.61 Å in all cases studied. This is one of the experimentally reported situations [15] for Mn on Cu_2N/Cu(001). In our supercell calculations, chains are periodically arranged 7.2 Å apart from

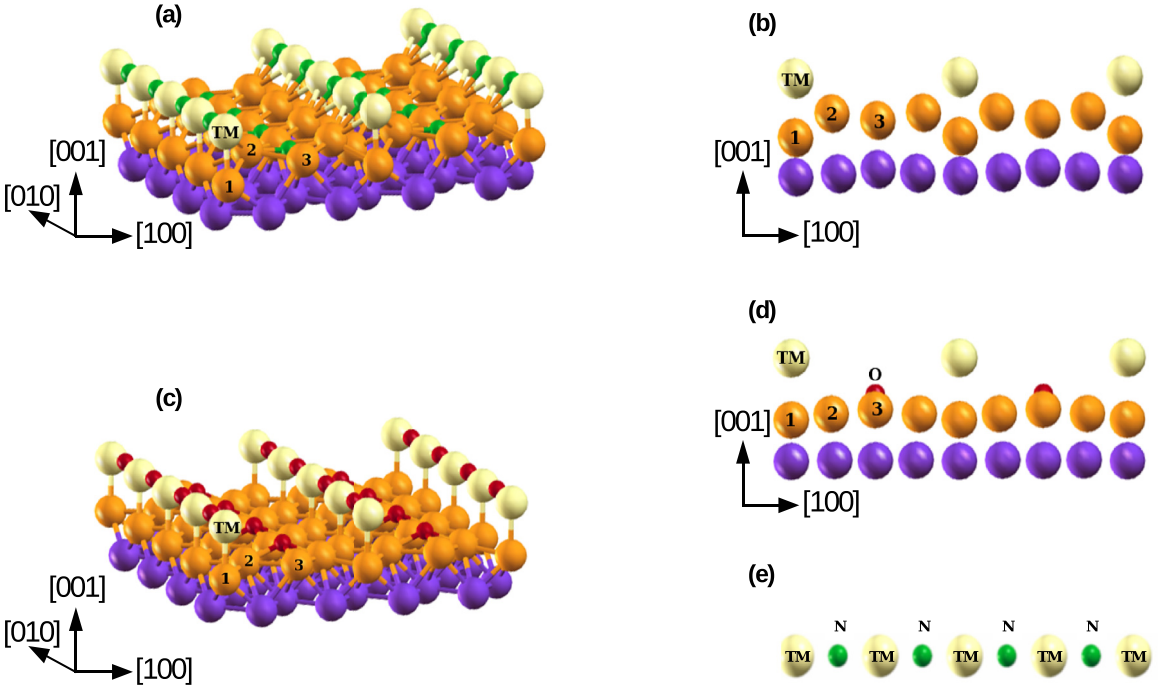

FIG. 1. (Color online) Relaxed structures of supported 3*d* chains. (a) and (c) Full views of the resulting diatomic chains on Cu_2N/Cu(001) and Cu_2O/Cu(001), respectively. (b) and (d) Lateral views of panels (a) and (c) with the diatomic chains perpendicular to the plane. (e) Diatomic TM-N unsupported chain. N and O atoms are depicted by small, dark spheres (respectively green and red online). White spheres indicate 3*d* TM atoms (yellow online), and light or dark gray spheres indicate surface or subsurface Cu atoms, respectively (orange and violet online).

each other [see Figs. 1(b) and 1(d)]. We checked that the interchain magnetic interaction energy at this distance and between chains on opposite sides of the slabs is of the order of 2 meV, at least one order of magnitude smaller than the intrachain magnetic interaction energy. The positions of all atoms in the supercells are allowed to move until forces on each atom are under 0.04 eV/Å.

III. CALCULATION RESULTS

Relaxed TM chains on Cu_2N/Cu(001) and on Cu_2O/Cu(001) are shown schematically in Figs. 1(a)–1(d). No relevant differences in the relaxation of the chains are observed among the different 3*d* fillings. The N or O atoms, which are between two 3*d* atoms, change significantly their vertical distance to the monolayer, relaxing outwards and forming nearly linear diatomic chains together with the 3*d* atoms. For the case of Cu_2N/Cu(001), this is in agreement with previous results [16]. However, the Cu_2N and Cu_2O monolayers relax slightly differently in the presence of TM chains as can be seen in Figs. 1(a)–1(d). The main difference is that the distance between the *sp* atom, which forms the diatomic chains, and the neighboring Cu atom, indexed as Cu(2), is larger in the Cu_2O monolayer than in Cu_2N monolayer. The principal structural properties of the systems are summarized in Table I. In the last section, we relate the magnetic behavior of the systems with their structural properties.

We consider only collinear ferromagnetic (FM) and antiferromagnetic (AFM) intrachain configurations for each system. To analyze the evolution of the magnetic ground state as a function of *d*-band filling, we calculate the total energy difference ΔE between the AFM and FM solutions. If this difference is negative the magnetic ground state is AFM; if not, it is FM. The results obtained for the deposited chains are shown in Fig. 2. It is seen that both substrates give rise, with minor differences, to the same magnetic trends and that the only chains which are ferromagnetic after adsorption are Cr chains.

In the resulting diatomic chains one can argue that there are, in principle, contributions through the *sp* bridging atoms and contributions mediated by the substrate. In order to understand the role played by the substrate and by the *d* filling, we also studied unsupported linear chains TM-O and TM-N [as an example, see Fig. 1(e) depicting a TM-N chain].

TABLE I. Structural properties of the systems. d_{X-TM} is the distance between the *X* atom (N, O) and the deposited TM atom, $d_{TM-Cu(1)}$ is the distance between the TM atom and the underlying Cu, and $d_{TM-Cu(3)}$ is the distance between the TM atom and the Cu(3) atom. $d_{X-Cu(2)}$ is defined as the distance between the *X* atom (N, O) and the Cu(2) atom. The values are given in Å.

	Ti	V	Cr	Mn	Fe	Co	Cu_2N
d_{N-TM}	1.90	1.86	1.81	1.81	1.81	1.81	
$d_{TM-Cu(1)}$	2.41	2.35	2.35	2.38	2.33	2.28	
$d_{TM-Cu(3)}$	4.01	3.98	3.99	4.02	4.03	4.00	
$d_{N-Cu(2)}$	2.91	2.55	2.18	2.10	2.01	2.04	1.82
	Ti	V	Cr	Mn	Fe	Co	Cu_2N
d_{O-TM}	1.90	1.87	1.82	1.84	1.83	1.81	
$d_{TM-Cu(1)}$	2.41	2.44	2.48	2.43	2.37	2.33	
$d_{TM-Cu(3)}$	4.12	4.15	4.16	4.14	4.11	4.06	
$d_{O-Cu(2)}$	3.15	3.13	3.01	3.04	2.91	2.66	1.95

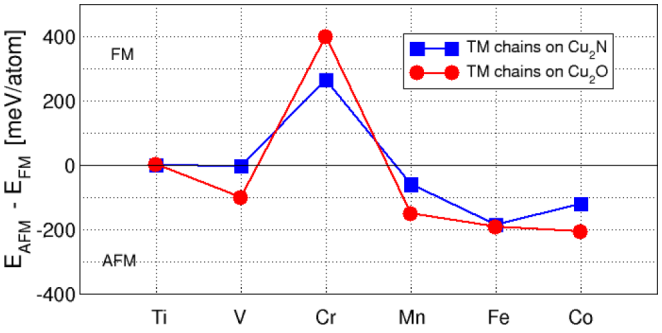

FIG. 2. (Color online) Difference in total energy between the AFM and FM collinear chain configurations as a function of 3*d* filling for TM chains adsorbed on Cu_2N/Cu(001) (squares, blue online) and Cu_2O/Cu(001) (circles, red online).

In Fig. 3 we show the evolution of these ground states for the two types of unsupported chains as a function of *d* filling. For oxygen bridging, the TM atoms present the same behavior as the deposited chains on Cu_2O, while in the case of the nitrogen bridge the strongest ferromagnetic ground state is given for Mn and not for Cr as for the TM-O chains.

Because N ($2s^2 2p^3$) has one less valence *p* electron than oxygen ($2s^2 2p^4$), the transitions from the FM to AFM ground state shown in Fig. 3 demonstrate that, for an unsupported system, they happen when the total number of valence electrons increases from 12 to 13 (Mn for O and Fe for N). If one relates the magnetic order to the filling of the 3*d* bands it is somehow natural to see a left shift of the curves when changing the *sp* atom from O to N.

The dependence of the total magnetic moment of the supported and unsupported chains on the 3*d* filling is shown in Fig. 4. For the unsupported chains with O [red circles in Fig. 4(b)], the evolution of the magnetic moment corresponds to a perfect splitting between the 3*d*-up and 3*d*-down bands. In other words, in this case, the crystal splitting is smaller than the effective Hund intra-atomic interaction *I*. From Ti to Mn, the magnetic moment increases from $2\mu_B$ to $5\mu_B$ and then

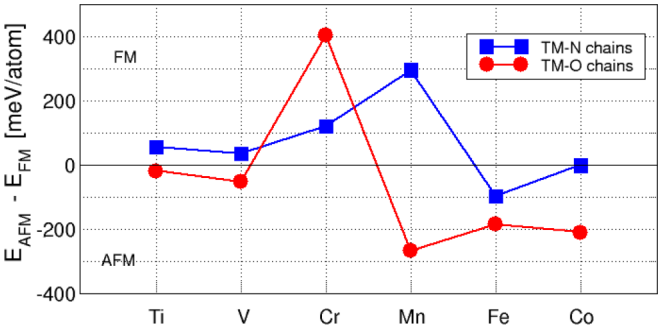

FIG. 3. (Color online) Difference in total energy between the AFM and FM collinear chain configurations as a function of *d* filling for linear diatomic unsupported chains. The results for the TM-N chains are shown represented by squares (blue online) and for TM-O by circles (red online).

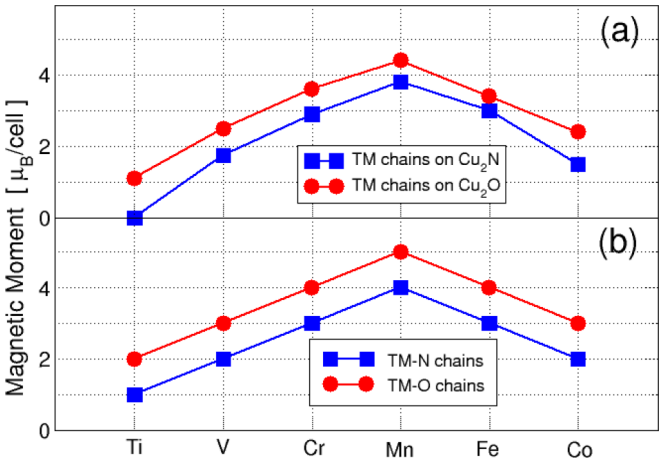

FIG. 4. (Color online) Total magnetic moments per unit cell for (a) TM metal chains supported on $Cu_2N/Cu(001)$ (blue squares) and $Cu_2O/Cu(001)$ (red circles) and (b) unsupported TM-N (blue squares) and TM-O (red circles) chains.

decreases with the number of valence electrons. The magnetic moment of the unsupported TM-N chains is similar if we take into account that there is one less electron available [blue squares in Fig. 4(b)]. The difference is that the maximum magnetic moment is only $4\mu_B$, corresponding to a crossover between the down and up bands. The dependence of the magnetic moments of the supported chains with the $3d$ filling is shown in Fig. 4(a). The main difference is the systematic decrease of the magnetic moments due to the hybridization with the substrate in the Cu_2N case.

The evolution of the occupation of the spin-polarized bands are shown in Figs. 5 and 6 for the TM-N and TM-O unsupported chains, respectively. In both cases, from Ti to Mn, the above-mentioned saturation of the magnetic moments is in agreement with the position of the $3d$ spin-down bands above the Fermi level (lower panels in Figs. 5 and 6). The decrease of the magnetic moment of Fe and Co is a consequence of the filling of the spin-down bands.

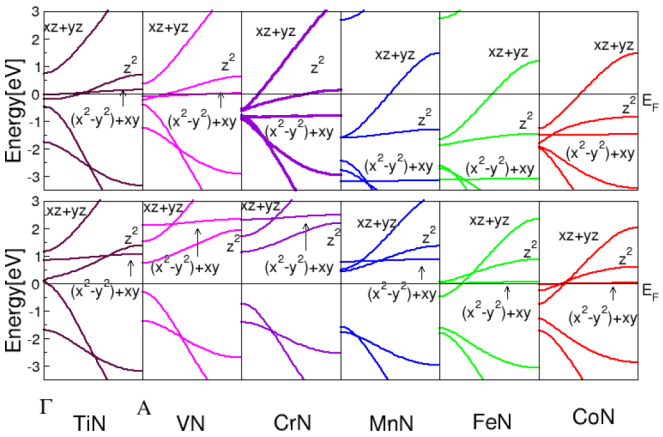

FIG. 5. (Color online) Magnetic band structures around the Fermi level for the TM-N unsupported chains calculated in the ferromagnetic configuration using the WIEN2k code. The upper and the lower panels show the up and down bands, respectively.

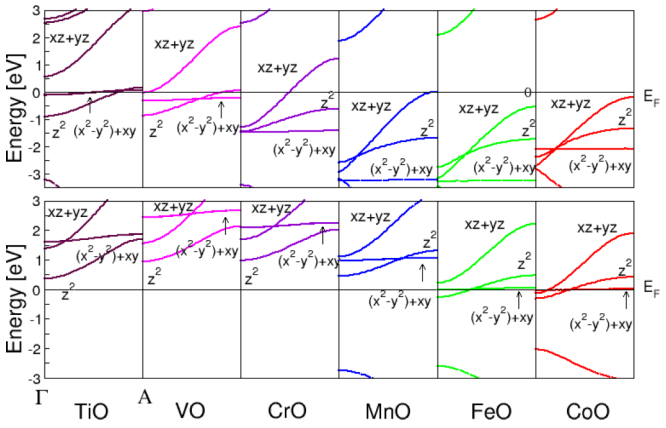

FIG. 6. (Color online) Magnetic band structures around the Fermi level for the TM-O unsupported chains calculated in the ferromagnetic configuration by using the WIEN2k code. The upper and the lower panels show the up and down bands, respectively.

The AFM solution for the Mn chains on $Cu_2N/Cu(001)$ (see Fig. 2) is in agreement with other experimental [15,16] and theoretical [26,27] works. The estimated experimental effective exchange interaction is $J = 6$ meV. Assuming a Heisenberg Hamiltonian, we estimate a value of 4.8 meV from the calculated energy difference $\Delta E = 2S^2 J = 60$ meV and a spin $S = 5/2$. The AFM ground state for Fe chains agrees with the ground state found for Fe dimers and trimers calculated by using GGA + U [31,32] by Nicklas *et al.* [33]. Their estimate of the effective interaction for the dimer, $J = 28$ meV, and trimer, $J = 34$ meV, are in good agreement with the $J = 40$ meV estimated by ourselves from the energy difference $\Delta E = 180$ meV and a spin $S = 3/2$.

We also checked that the use of GGA + U instead of plain GGA has a limited effect on our results. By using $U = 5$ eV for Cr and Mn and $U = 2$ eV for Fe, we compared the total energy differences between the AFM and FM configurations, ΔE, for these TM chains adsorbed on $Cu_2N/Cu(001)$. We obtained in the case of Cr that ΔE is 275 meV/atom with GGA and 260 meV/atom with GGA + U, for Mn −60meV/atom and −40 meV/atom, and for Fe −185 meV/atom and −175 meV/atom.

In the next section we consider a simple Hamiltonian that allows us to understand the FM to AFM transition in the unsupported TM-N and TM-O chains. The different behavior between the supported and unsupported chains will be discussed in Sec. V.

IV. EXCHANGE MODEL

As expected, the three bands close to the Fermi level have a strong $3d$ character of the TM (see Figs. 5 and 6). With the z axis of the local coordinate system along the chains, these bands correspond to the d_{z^2} nondegenerate band ($m = 0$), the doubly degenerate bands with d_{xz} and d_{yz} character ($m = \pm 1$), and the doubly degenerate flat bands with $d_{x^2-y^2}$ and d_{xy} character ($m = \pm 2$). The difference in electronegativity between the two ligands is clearly reflected if we compare the spin-down bands (lower panels) of both systems. On the energy scale of the band-structure plots, the low-energy bonding bands

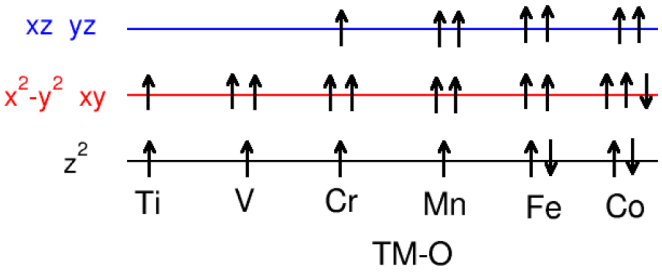

FIG. 7. (Color online) Proposed filling of the 3*d* orbitals for the TM-O unsupported chains used to calculate the energy differences presented in Fig. 8.

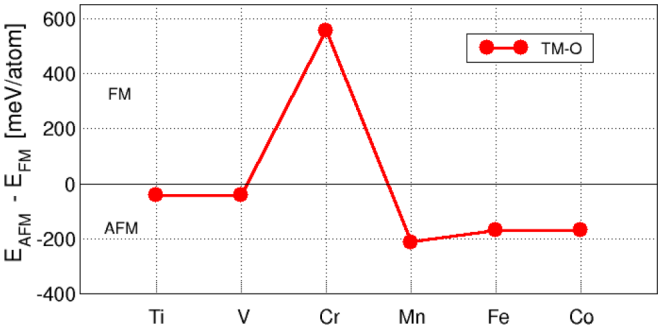

FIG. 8. (Color online) Energy differences between the AFM and FM chain configurations as a function of *d* filling for linear TM-O diatomic unsupported chains. The differences where calculated by using Eqs. (1) to (4), the orbital occupancies sketched in Fig. 7, $U = 6$ eV, $U' = 4$ eV, $I = 2.5$ eV, $t_0 = 0.25$ eV, and $t_1 = 0.60$ eV.

of N character are more visible (closer to the Fermi level) than those of O character. This is in agreement with the expected more-ionic character of the oxygen bonds.

Having this in mind, we can assume that two of the original valence electrons of the TM go to the O atom and the remaining valence electrons fill the 3*d* orbitals. Looking carefully at the upper panel of Fig. 6 it seems clear that the first electron goes to the nondegenerate z^2 up orbital and the subsequent ones to the double degenerate xz/yz and $x^2 - y^2/xy$ up orbitals. A schematic picture representing the filling of the 3*d* bands is shown in Fig. 7.

To relate the filling of these bands to the energy differences obtained for the unsupported TM-O chains presented in Fig. 3, we considered a tight-binding Hamiltonian for the effective magnetic orbitals centered on the TM atoms. The hopping integrals are treated as a perturbation, in the spirit of the kinetic or Kugel–Khomskii models [4,34–37].

For a perfectly straight chain, symmetry reasons allow to consider separately each one of the 3*d* bands. In the case of the d_{z^2} character, only the level occupation with one electron is of interest; namely, the half-filled situation. In the case of the double degenerate states with d_{xz} and d_{yz} symmetries, there are three occupations to be considered: $\frac{1}{4}$, $\frac{1}{2}$, and $\frac{3}{4}$. We do not consider the contributions to the magnetic order of the double degenerate orbitals with $d_{x^2+y^2}$ and d_{xy} symmetries. The reason is that the corresponding bands (see Figs. 5 and 6) are extremely flat and the hopping integrals are negligibly small.

The expressions for the difference in energy between antiferromagnetic and ferromagnetic configurations of the model system, $\Delta E = E_{\mathrm{AFM}} - E_{\mathrm{FM}}$, are obtained by using second-order perturbation theory. For the z^2 orbital and filling $\frac{1}{2}$, the energy difference is the simple expression for kinetic exchange :

$$\Delta E^0_{1/2} = -\frac{4\,t_0^2}{U}. \tag{1}$$

For the double-degenerate orbitals xz/yz and filling $\frac{1}{4}$, the energy difference is

$$\Delta E^1_{1/4} = \frac{4\,I\,t_1^2}{U'(U'-I)}. \tag{2}$$

For filling $\frac{1}{2}$, the energy difference is

$$\Delta E^1_{1/2} = -\frac{4\,t_1^2}{U+I}. \tag{3}$$

Finally, for filling $\frac{3}{4}$, the energy difference is

$$\Delta E^1_{3/4} = \frac{4\,I\,t_1^2}{U'(U'-I)}. \tag{4}$$

In Eqs. (1)–(4), t_0 and t_1 are respectively the effective hopping integrals between two $m = 0$ or two $m = \pm 1$ orbitals, U is the Coulomb repulsion between two electrons in the same *d* orbital, U' is the corresponding repulsion between electrons in different *d* orbitals in the same atom, and I is the intra-atomic Hund exchange interaction [38].

The energy differences calculated with these expressions and the orbital occupancies sketched in Fig. 7 are shown in Fig. 8. They have been calculated with a single set of reasonable values: $U = 6$ eV, $U' = 4$ eV, $I = 2.5$ eV, $t_0 = 0.25$ eV, and $t_1 = 0.60$ eV.

The qualitative agreement with the calculated energy differences for the TM-O chain presented in Fig. 3 is remarkably good.

In Table II we show the contributions of the different orbitals to the energy difference. The small AFM contribution of the z^2 orbital is due to the small dispersion of the bands (see Fig. 6) and the relative high value of the repulsive Coulomb interaction. The enhanced AFM character for Mn is a consequence of the synergic contribution of the z^2 and the xz/yz orbitals. The FM ground state for Cr is a consequence of the relatively large FM contribution of the double-degenerate xz/yz orbital with filling $\frac{1}{4}$ in comparison with the AFM contribution of the z^2 orbital. The condition that should be

TABLE II. Contributions to the energy difference between the AFM and the FM order of the different orbitals as a function of *d* filling for the linear TM-O diatomic unsupported chains. The differences where calculated by using Eqs. (1) to (4), the orbital occupancies sketched in Fig. 7, and the numerical values reported in the text and are given in meV.

	Ti	V	Cr	Mn	Fe	Co
xz/yz			600	−169	−169	−169
$x^2 - y^2/xy$						
z^2	−42	−42	−42	−42		

fulfilled by the tight-binding parameters for a stabilization of the FM ground state in the case of Cr ($\Delta E^1_{1/4} + \Delta E^0_{1/2} > 0$) can be written as

$$\left(\frac{t_1}{t_0}\right)^2 > \frac{U'(U'-I)}{IU}. \quad (5)$$

On the one hand, in order to have a FM ground state, a strictly nonzero value for the effective Hund interaction I is needed. On the other hand, the relatively large dispersion of the xz/yz bands with respect to the z^2 bands ($t_1 \gg t_0$) makes the stabilization of the FM ground state a robust result against other choices of the effective Coulomb interactions U and U'. It is interesting to note that, in the case of Cr, the ground state stabilized by the degenerate orbitals xz/yz corresponds to a FM spin order and an AFM-orbital order, i.e., the occupied orbitals are alternatively xz and the yz.

The case of unsupported TM-N chains is a little more complicated. If we fill with electrons the same energy scheme for the 3d orbitals as for the TM-O case (Fig. 7), we would correctly predict FM for Mn-N and a transition to AFM for Fe-N. However, the same scheme will incorrectly predict a small stabilization of the AFM ground state for Ti, V, and Cr when the *ab initio* calculations give a FM ground state. The reasons can be seen in the magnetic band structure of Fig. 5: the filling of the 3d bands is not as clear as in the case of the TM-O chains; the successively added electrons spread over the bands and the rigid energy levels sketched in Fig. 7 do not strictly correspond to the actual band filling. In particular, the AFM solution is the preferred magnetic order for a single occupied nondegenerate band. The spread of the 3d electrons between the different orbitals and the departure from half filling could be at the origin of the stabilization of the FM order for Ti, V, and Cr.

V. DISCUSSION AND CONCLUSIONS

The exchange model presented in the preceding section has been used to explain the energy difference for the unsupported chains. The similarity of the energy difference and magnetic moments plots for the supported and unsupported chains in the TM-O case makes us believe that the same arguments can be used to explain the magnetic order for the supported TM-O chains.

The striking result is that the supported TM-N chains show a magnetic trend similar to that for the supported TM-O chains. A possible explanation could be that there is a small but significative charge transfer between the chains and the substrate that would explain why the chains behave as deposited on Cu_2O even though they are deposited on Cu_2N.

This argument is supported by the electronic density plots that we show in Fig. 9. One can see that the copper atom labeled as Cu(2) is closer to the neighboring N atom than the same Cu(2) atom is to the corresponding O atom. This indicates a less-important bonding effect for the latter substrate. Thus, Cu(2) contributes to charge transfer from the substrate to the chains and, in the presence of the Cu_2N, it would help to transform the diatomic TM-N chains into TM-O-like chains. This can also be inferred from Table I when comparing the distance between Cu(2) and the nearest sp atoms of the chains for both cases under study. The distance N-Cu(2) is systematically smaller than the distance O-Cu(2), in agreement with the electron transfer in the former case.

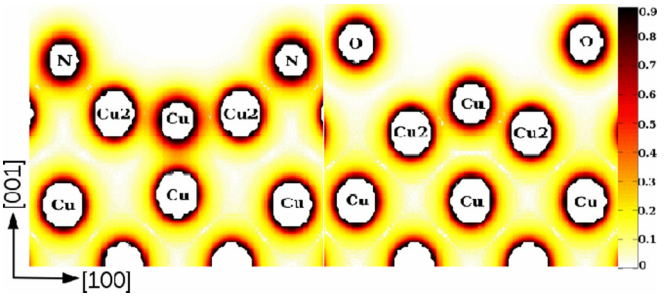

FIG. 9. (Color online) Charge density plots on a plane perpendicular to the (a) TM-N and (b) TM-O chains and containing an sp atom of the diatomic nanostructures.

In conclusion, in this work we studied the influence of a covalent ultrathin film on the magnetic interactions within adsorbed 3d transition-metal chains, when this film separates the adsorbed nanostructures from a metallic substrate. We focused on the case of a Cu_2N monolayer as decoupling layer from Cu(001). This decoupling layer has been the object of several experimental as well as theoretical works. Among the possible adsorption arrangements for TM chains, we studied the particular one which gives rise to the appearance of diatomic TM-N chains after relaxation of the systems. To understand the role played by the substrate we also considered a similar substrate where the decoupling monolayer is Cu_2O. We performed DFT calculations for 3d TM atoms going from Ti to Co. Both substrates give rise to the same magnetic trends; the only chains which present ferromagnetic order after adsorption are Cr chains.

By performing similar calculations for unsupported chains and introducing a tight-binding-model Hamiltonian based on physically reasonable assumptions we were able to reproduce the magnetic trends obtained from the DFT calculations. It was possible to identify the orbital occupancies which give rise to different magnetic ground states as a function of d filling in the resulting diatomic chains and to understand the antiferromagnetic-to-ferromagnetic transition that takes place at the d filling corresponding to Cr.

We expect that it should be possible to obtain similar behavior for other decoupling films by properly engineering these films and selecting suitable adsorption sites for the atoms intended to build a supported nanostructure.

ACKNOWLEDGMENTS

We acknowledge fruitful discussions with Guillaume Radtke. M.A.B. is supported and M.C.U. and A.M.L. are partially supported by CONICET and belong to the Institute of Nanoscience and Nanotechnology (INN) of the Atomic Energy Agency (CNEA), Argentina. This work was partially funded by the grants PIP00273 (CONICET), UBACYT-W354 (UBA), PICT-2011-1187 (ANPCyT), and PRH074 (ANPCyT).

[1] M. Jaime, V. F. Correa, N. Harrison, C. D. Batista, N. Kawashima, Y. Kazuma, G. A. Jorge, R. Stein, I. Heinmaa, S. A. Zvyagin, Y. Sasago, and K. Uchinokura, Phys. Rev. Lett. **93**, 087203 (2004).

[2] I. S. Camara, R. Gautier, E. LeFur, J. C. Trombe, J. Galy, A. M. Ghorayeb, and A. Stepanov, Phys. Rev. B **81**, 184433 (2010).

[3] G. Radtke, A. Saúl, H. A. Dabkowska, G. M. Luke, and G. A. Botton, Phys. Rev. Lett. **105**, 036401 (2010).

[4] A. Saúl and G. Radtke, Phys. Rev. Lett. **106**, 177203 (2011).

[5] S. V. Streltsov and D. I. Khomskii, Phys. Rev. B **86**, 064429 (2012).

[6] G. Radtke, A. Saúl, Y. Klein, and G. Rousse, Phys. Rev. B **87**, 054436 (2013).

[7] Y. Endoh, G. Shirane, R. J. Birgeneau, P. M. Richards, and S. L. Holt, Phys. Rev. Lett. **32**, 170 (1974).

[8] I. U. Heilmann, G. Shirane, Y. Endoh, R. J. Birgeneau, and S. L. Holt, Phys. Rev. B **18**, 3530 (1978).

[9] M. Hase, I. Terasaki, and K. Uchinokura, Phys. Rev. Lett. **70**, 3651 (1993).

[10] M. Azuma, Z. Hiroi, M. Takano, K. Ishida, and Y. Kitaoka, Phys. Rev. Lett. **73**, 3463 (1994).

[11] Y. Ueda, Chem. Mater. **10**, 2653 (1998).

[12] P. Gambardella, A. Dallmeyer, K. Maiti, M. C. Malagoli, W. Eberhardt, K. Kern, and R. C. Carbone, Nature (London) **416**, 301 (2002).

[13] A. Vindigni, A. Rettori, M. G. Pini, C. Carbone, and P. Gambardella, Appl. Phys. A: Mater. Sci. Process. **82**, 385 (2006).

[14] A. J. Heinrich, J. A. Gupta, C. P. Lutz, and D. M. Eigler, Science **306**, 466 (2004).

[15] C. Hirjibehedin, C. Lutz, and A. Heinrich, Science **312**, 1021 (2006).

[16] C. F. Hirjibehedin, Chiung-Yuan Lin, A. F. Otte, M. Ternes, C. P. Lutz, B. A. Jones, and A. J. Heinrich, Science **317**, 1199 (2007).

[17] H. Brune, Science **312**, 1005 (2006).

[18] H. Brune and P. Gambardella, Surf. Sci. **603**, 1812 (2009).

[19] Kun Tao, V. S. Stepanyuk, W. Hergert, I. Rungger, S. Sanvito, and P. Bruno, Phys. Rev. Lett. **103**, 057202 (2009).

[20] S. Loth, K. von Bergmann. M. Ternes, A. F. Otte, C. P. Lutz, and A. J. Heinrich, Nat. Phys. **6**, 340 (2010).

[21] A. A. Khajetoorians, J. Wiebe, B. Chilian, and R. Wiesendanger, Science **332**, 1062 (2011).

[22] A. A. Khajetoorians, B. Baxevanis, C. Hbner, T. Schlenk, S. Krause, T. O. Wehling, S. Lounis, A. Lichtenstein, D. Pfannkuche, J. Wiebe, and R. Wiesendanger, Science **339**, 55 (2013).

[23] S. Loth, S. Baumann, C. P. Lutz, D. M. Eigler, and A. J. Heinrich, Science **335**, 196 (2012).

[24] B. Bryant, A. Spinelli, J. J. T. Wagenaar, M. Gerrits, and A. F. Otte, Phys. Rev. Lett. **111**, 127203 (2013).

[25] Y. Mokrousov, G. Bihlmayer, S. Blügel, and S. Heinze, Phys. Rev. B **75**, 104413 (2007).

[26] A. N. Rudenko, V. V. Mazurenko, V. I. Anisimov, and A. I. Lichtenstein, Phys. Rev. B **79**, 144418 (2009).

[27] M. A. Barral, R. Weht, G. Lozano, and A. M. Llois, Phys. B (Amsterdam, Neth.) **398**, 369 (2007).

[28] M. C. Urdaniz, M. A. Barral, and A. M. Llois, Phys. Rev. B **86**, 245416 (2012).

[29] P. Blaha, K. Schwarz, G. K. H. Madsen, D. Kvasnicka, and J. Luitz, *WEIN2k, an Augmented Plane Wave + Local Orbitals Program for Calculating Crystal Properties* (Techn. Universitat Wien, 2001).

[30] J. P. Perdew and Y. Wang, Phys. Rev. B **45**, 13244 (1992).

[31] V. I. Anisimov, I. V. Solovyev, M. A. Korotin, M. T. Czyzyk, and G. A. Sawatzky, Phys. Rev. B **48**, 16929 (1993).

[32] A. I. Liechtenstein, V. I. Anisimov, and J. Zaanen, Phys. Rev. B **52**, R5467(R) (1995).

[33] J. W. Nicklas, A. Wadehra, and J. W. Wilkins, J. Appl. Phys. **110**, 123915 (2011).

[34] K. I. Kugel and D. I. Khomskii, Sov. Phys. Usp. **25**, 231 (1982).

[35] A. Saúl and G. Radtke, Phys. Rev. B **89**, 104414 (2014).

[36] V. V. Mazurenko, F. Mila, and V. I. Anisimov, Phys. Rev. B **73**, 014418 (2006).

[37] A. A. Tsirlin, O. Janson, and H. Rosner, Phys. Rev. B **84**, 144429 (2011).

[38] Only U' appears in Eqs. (2) and (4) because both lowest-energy FM and AFM configurations present AFM-orbital ordering, i.e., the electrons occupy different orbitals in different atoms. As for symmetry reasons, there is no interorbital hopping (between xz and yz orbitals in different sites), the repulsion energy of the virtual state is always U' instead of U: $E_{\mathrm{FM}} = 2\varepsilon_d - 4t_1^2/(U' - I)$ and $E_{\mathrm{AFM}} = 2\varepsilon_d - 4t_1^2/U'$, where ε_d is the on-site energy of a d orbital. The other AFM state, with the electrons in the same orbital at different sites, has a higher energy, $2\varepsilon_d - 4t_1^2/U$, than the one with AFM-orbital ordering.